Measurements of a Barotropic Planetary Vorticity Mode in an Eddy-Resolving Quasi-geostrophic Model Using Acoustic Tomography*

WENDY B. LAWRENCE

Joint Masters Program in Oceanographic Engineering at the Massachusetts Institute of Technology and the Woods Hole Oceanographic Institution, Woods Hole, Massachusetts

JOHN L. SPIESBERGER

Woods Hole Oceanographic Institution, Woods Hole, Massachusetts

(Manuscript received 26 August 1988, in final form 19 December 1988)

ABSTRACT

An acoustic source and receiver are placed at 800 m depth and are separated by 4000 km in a two-layer, steady-wind driven, flat bottom eddy-resolving quasi-geostrophic circulation model. Time series of sea surface elevation and upper and lower layer meridional currents are generated for comparison against a series of acoustic travel time. The spectra of the time series exhibit a broad mesoscale peak near a period of 40 days. The spectrum of the acoustic travel time contains a significant peak, which is not present in the spectra of the point measurements, due to a resonant barotropic oscillation with a period of 29.0 days. In this numerical model, basin-scale tomographic measurements are a useful method of sensing the large-scale resonant barotropic oscillations because the tomographic system attenuates the "noise" from the mesoscale.

1. Introduction

Resonant barotropic vorticity oscillations, associated with quasi-geostrophic (QG) theory, are notoriously difficult to observe in the ocean. For example, Luther (1982) presents evidence from 2 to 7 years of sea level data from some Pacific islands that suggests the presence of one or more barotropic planetary oscillations in the 4 to 6 day period band. It is apparent that large-scale measurements over lengthy durations will be necessary in order to observe these waves without ambiguity.

The capability of receiving long-range sound transmissions in the ocean implies that acoustic methods may be well-suited for the study of such large-scale motions. In particular, basin-scale tomographic arrays may provide the coverage over sufficient time periods as well as the sensitivity needed to resolve the modes (Bushong 1987; Spiesberger et al. 1989a).

In this study, we investigate whether the analysis of the travel time fluctuations of tomographic transmission exhibits large-scale barotropic planetary oscillations in a QG model which contains both large-scale and mesoscale disturbances. We use four years of data from the two-layer, steady-wind driven, flat bottom eddy-resolving general circulation model in which Miller et al. (1987) detected barotropic-mode resonances. A tomographic array is placed in the model and a time series of travel time is computed. This series is compared with the contemporaneous series of sea surface elevation and current. The analysis demonstrates that acoustic tomography provides an effective method of detecting barotropic modes in a QG model.

Section 2 describes how the tomographic travel times are affected by fluctuations of the temperature, pressure and currents in a QG model. Section 3 describes the response of the acoustic travel times due to singlet free solutions of the QG equations. Section 4 describes the geometry and location of the tomographic section in the QG model. Section 5 discusses the time series analysis of the tomographic travel times, the sea surface elevation and the currents. A discussion follows in section 6.

2. The forward problem

a. Definitions

The change in the travel time along an acoustic ray path Γ_0 at geophysical time t is approximately given by

$$\delta T(t) = -\int_{\Gamma_0} \frac{1}{c_0^2(z_{\text{ray}})}\left[\eta \frac{\partial c_p}{\partial z} + \gamma \delta p + \vec{u}\cdot\mathbf{s}\right] ds, \quad (1)$$

where the reference sound speed profile is $c_0(z)$ and the increment of ray path is ds with unit vector $\mathbf{s}$ (Munk

* Contribution Number 6942 from the Woods Hole Oceanographic Institution.

Corresponding author address: Dr. John Spiesberger, Woods Hole Oceanographic Institution, Woods Hole, MA 02543.

et al. 1981). A Cartesian coordinate system is adapted where (x, y, z) is positive (eastward, northward, upward) with unit vector $(\mathbf{i}, \mathbf{j}, \mathbf{k})$. Vectors are denoted by arrows.

The travel time is affected by three processes. One, the vertical displacement of water (positive up), $\eta(\vec{s}, t)$, approximately changes the in situ speed of sound by

$$\delta c(\vec{s}, t) \approx \eta(\vec{s}, t) \frac{\partial c_p(\vec{s}, t)}{\partial z}, \tag{2}$$

where the potential sound speed is c_p (Munk et al. 1981). Two, changes in the hydrostatic pressure, $\delta p(\vec{s}, t)$, which arise from surface displacements, alter the in situ sound speed by

$$\delta c(\vec{s}, t) \approx \gamma \delta p(\vec{s}, t), \tag{3}$$

where the proportionality constant, γ, is approximately 1.682×10^{-6} m s^{-1} Pa^{-1} (Munk 1974). Three, the projection of the horizontal current,

$$\vec{u}(\vec{s}, t) = u(\vec{s}, t)\mathbf{i} + v(\vec{s}, t)\mathbf{j}, \tag{4}$$

onto the unit vector, $\mathbf{s}$, along the ray path also affects the travel time. The position of a ray is given by

$$\vec{s} = x_{\text{ray}}\mathbf{i} + y_{\text{ray}}\mathbf{j} + z_{\text{ray}}\mathbf{k}.$$

Vertical currents are negligible in this study.

b. Relation to the quasi-geostrophic model

The quantities computed in the quasi-geostrophic model are shown in Fig. 1. Under rigid-lid dynamics, the vertical displacement of water parcels is determined entirely by the baroclinic mode, so that

$$\eta(x, y, z, t) = \begin{cases} \dfrac{-h(x, y, t)z}{H_1}, & z > -H_1 \text{ (upper layer)} \\ \dfrac{h(x, y, t)(H + z)}{H - H_1}, & z \leqslant -H_1 \text{ (lower layer).} \end{cases} \tag{5}$$

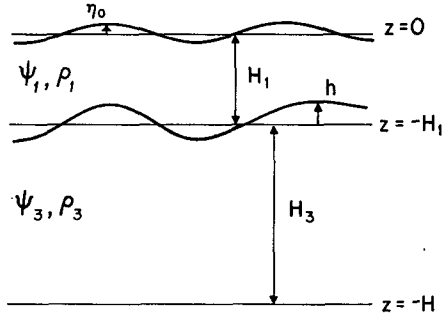

FIG. 1. Definition figure of the quantities computed in the quasi-geostrophic model. The undisturbed depth is H and the undisturbed layer thicknesses are H_1 (1000 m) and H_3 (4000 m). The interface displacement is h and the surface displacement is η_0 (both positive up). The streamfunction in the upper and lower layers is ψ_1 and ψ_3, respectively. The densities in the layers are ρ_1 and ρ_3.

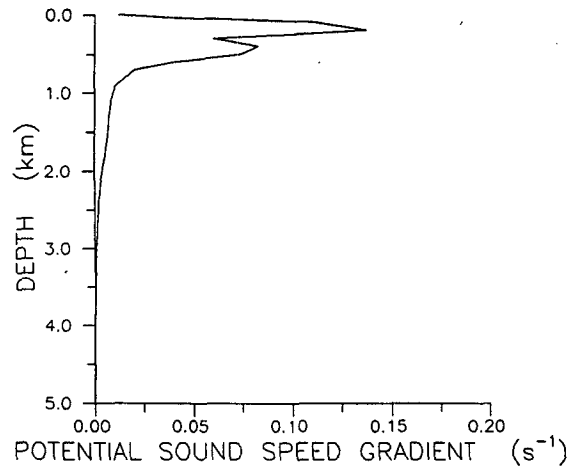

FIG. 2. The climatological potential sound speed gradient in the northeast Pacific near 30°N, 150°W.

The perturbation pressure is

$$\delta p(x, y, z, t) = \begin{cases} \rho_0 f_0 \psi_1(x, y, t), \\ \qquad z > -H_1 \text{ (upper layer)} \\ \rho_0 g \eta_0(x, y, t) + \rho_0 g' h(x, y, t), \\ \qquad z \leqslant -H_1 \text{ (lower layer),} \end{cases} \tag{6}$$

where the mean density is ρ_0, the Coriolis parameter is f_0 and the reduced gravity is

$$g' = \frac{g(\rho_3 - \rho_1)}{\rho_0}.$$

The interface displacement is given by

$$h(x, y, t) = \frac{f_0}{g'}(\psi_3(x, y, t) - \psi_1(x, y, t)), \tag{7}$$

(Holland 1978). The horizontal currents are given by

$$u_i(x, y, t) = -\frac{\partial \psi_i(x, y, t)}{\partial y}, \quad i = 1, 3,$$

$$v_i(x, y, t) = \frac{\partial \psi_i(x, y, t)}{\partial x}, \quad i = 1, 3. \tag{8}$$

Parameter values are $\rho_0 = 1000.0$ kg m^{-3}, $f_0 = 9.3 \times 10^{-5}$ s^{-1} and $g' = 0.02$ m s^{-2}. The origin of the coordinate system is the lower left hand corner of the model (Fig. 5).

The QG model does not include thermodynamics. Therefore, the potential sound speed gradient is taken from a climatological average in the northeast Pacific (Fig. 2). The gradient is small below a depth of about one kilometer because the ocean is nearly adiabatic in this region.

3. The forward problem for modes

Miller et al. (1987) demonstrate that the large-scale barotropic response in this QG model is dominated by

a summation of resonant Rossby (planetary) basin modes which are excited by the mesoscale turbulence of the free jet region. Solutions for inviscid, unforced, flat bottom, normal modes are given by

$$\psi_{nm}(x, y, t) = \mathrm{Re}\left\{A_{nm} \exp\left(i\frac{\beta x}{2\sigma_{nm}}\right) \sin\left(\frac{n\pi x}{L}\right) \times \sin\left(\frac{m\pi y}{L}\right) \exp(i\sigma_{nm}t)\right\}, \quad (9)$$

where A_{nm} is the amplitude coefficient ($m^2\ s^{-1}$), β is the gradient of the Coriolis parameter, L is the length of a side in the square basin, n, m are positive integers and $\mathrm{Re}\{x\}$ denotes the real part of x (Pedlosky 1979). The modal frequency is defined as

$$\sigma_{nm} = \beta \Big/ \left(\frac{2\pi}{L}\sqrt{n^2 + m^2}\right).$$

We seek to determine the travel time changes induced by the presence of individual modes excited at resonance. Since the travel time changes due to the pressure and temperature fluctuations associated with these modes are approximately an order of magnitude smaller than the fluctuations due to currents (Spiesberger et al. 1989a), Eq. (1) can be simplified to

$$\delta T(t) \approx -\frac{1}{{c_0}^2}\int_{\Gamma_0} \vec{u}\cdot \mathbf{s}\, ds, \quad (10)$$

where $\vec{u}$ is the current associated with the mode and the small variation of the sound speed is neglected. From Eqs. (8) and (9), the horizontal currents are

$$u(x, y, t) = -A_{nm}\left(\frac{m\pi}{L}\right)\cos\left(\frac{\beta x}{2\sigma_{nm}}\right) \times \cos\left(\frac{m\pi y}{L}\right)\sin\left(\frac{n\pi x}{L}\right)\cos(\sigma_{nm}t),$$

$$v(x, y, t) = A_{nm}\left\{\left(\frac{n\pi}{L}\right)\cos\left(\frac{\beta x}{2\sigma_{nm}}\right)\cos\left(\frac{n\pi x}{L}\right) - \left(\frac{\beta}{2\sigma_{nm}}\right)\sin\left(\frac{\beta x}{2\sigma_{nm}}\right)\sin\left(\frac{n\pi x}{L}\right)\right\} \times \sin\left(\frac{m\pi y}{L}\right)\cos(\sigma_{nm}t). \quad (11)$$

For a tomographic section oriented along a north–south direction, Eq. (10) yields

$$\delta T(t) \approx -\frac{1}{{c_0}^2}\int_{y_1}^{y_2} v(x, y, t)\, dy, \quad (12)$$

where y_1 and y_2 are the positions of the tomographic instruments.

4. Selection of section location

We want to place the tomographic array in a portion of the QG model that is representative of the northeast Pacific Ocean because this study is investigating the feasibility of utilizing a 3000 by 4000 km tomographic array in the northeast Pacific to search for such modes (Spiesberger et al. 1989a). Using Roden's section of the Pacific along 158°W as a reference, typical eddy-like features (wavelengths of 100 to 200 km) perturb the in situ sound speed by about 0.2 to 0.5 m s^{-1} at

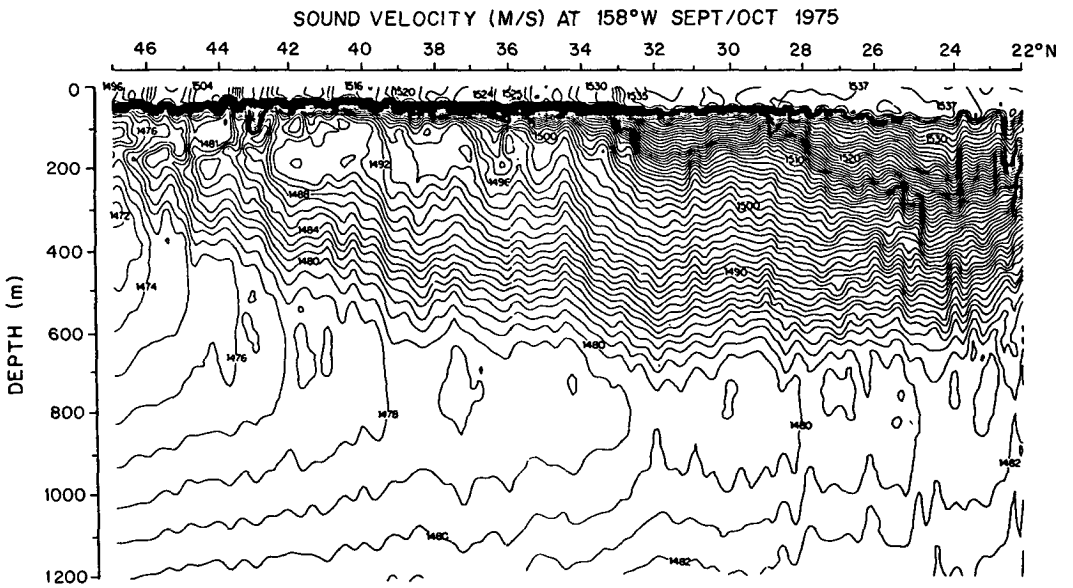

FIG. 3. A meridional section of sound speed in the northeast Pacific. Contour intervals are at 1 m s^{-1}. (Courtesy of G. I. Roden).

1000 m depth (Roden 1984). This corresponds to vertical displacements between 20 to 50 m (Fig. 3).

A significant problem associated with this particular QG model is the inadequate zonal penetration of both the eastward, midlatitude jet and of the abyssal mean and eddy kinetic energies (Schmitz and Holland 1982). The model's deep gyre extends to 1000–1200 km from the western boundary, whereas Worthington (1976) found that it extends to 2500 km in the North Atlantic. As a result, direct comparisons cannot be made between this model and the ocean at equivalent distances but a scaling factor must be used instead.

The QG sea surface elevation spectra levels are comparable to those of Pacific island stations only in the band between 25–50 days period (Miller et al. 1987). On either side of this band, the model spectral levels computed at a point just beyond the farthest eastward penetration of the free jet are roughly 10 dB lower than those computed by Luther (1982) for several stations.

Within this band, the resonant modes of larger amplitude typically have longer wavelengths in the north–south direction than in the east–west direction (see Table 1 in Miller et al. 1987). Thus, in order to maximize the response of the acoustic travel times, a north–south section is desirable. We focus our efforts on detecting mode 17 and place a 4000 km length section at x = 1160 km where the amplitude of the modal current in the meridional direction has a maximum value. Parameters for this mode are listed in Table 1. At this value of x in the QG model, the interface displacements (at 1000 m depth) are about 5 to 50 m which are comparable to Roden's observations (Fig. 4).

The position of the tomographic section with respect to the midlatitude jet is shown in Fig. 5. Measurements of the sea surface elevation and the meridional current are taken at y = 1500 km, and we refer to this location as station 1. The free jet meanders with time and its effects are felt approximately 600 km to either side of the midbasin point (y = 2000 km). On the average, the section is just within the farthest penetration of the jet, the region at which the eddies break off and travel toward the western boundary. Station 1 and the central portion of the tomographic section are influenced by eddy processes.

In summary, it is difficult to locate a region of this model whose eddy field is similar to that found in the northeast Pacific. However, we believe that the selected section is realistic enough so that a comparison of the tomographic and the point measurements provides a useful guide for further investigation.

TABLE 1. The scales of mode 17 in this QG model. The x and y wavelengths are indicated along with the rms values of the maximum sea surface displacement and the maximum meridional current.

(n, m)	Period (days)	λ_x (km)	λ_y (km)	Rms amplitude (cm)	Rms velocity (cm s^{-1})
5, 1	29.1	1600	8000	1.1	0.7

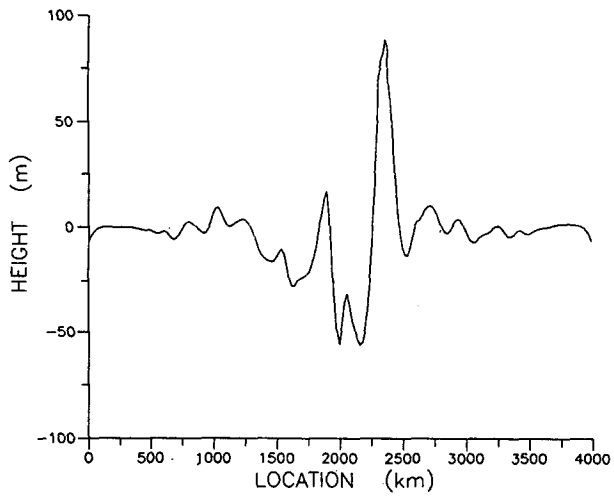

FIG. 4. Perturbation interface displacement of the two-layer QG model on day 4. The large-scale features in the middle of the section are due to the midlatitude free jet.

5. Spectral analysis

The QG model does not include the thermodynamic effects which give rise to a sound speed channel. So, the paths of three acoustic rays are traced through a climatological sound speed profile in the northeast Pacific at the same location at which the potential sound speed gradient is computed (Fig. 2). The source and receiver are at depths of 800 m and are separated by 4000 km (Fig. 5). The angles of the rays at the source (with respect to the horizontal) are 11.7°, 6.3° and 2.1°, and their upper turning depths are 154 m, 447 m and 638 m, respectively. The travel time series for each ray is computed from four years of statistically steady state streamfunction values which are sampled at 4-day intervals in the QG model by use of Eq. (1). The travel time series for the 11.7° ray is detrended with a ramp (Fig. 6). Time series are recorded for the sea surface elevation along with the upper and lower layer meridional currents for comparison against the series of the detrended travel time for the 11.7° ray (Fig. 7). The fluctuations of sea level and meridional current have a predominant period of 40–45 days. A dominant period is not visually evident in the travel time fluctuations.

The power spectral density levels are computed by dividing each time series into four non-overlapping segments, each of which has a duration of approximately one year. A Bartlett window is applied to the data, so the spectral estimates are chi-squared random variables with 12 degrees of freedom (Jenkins and Watts 1968). The highest sidelobe level for this window is −25 dB (Oppenheim and Schafer 1975).

Within the band of interest (25–50 days), the sea level and current spectra are similar in shape (Fig. 8).

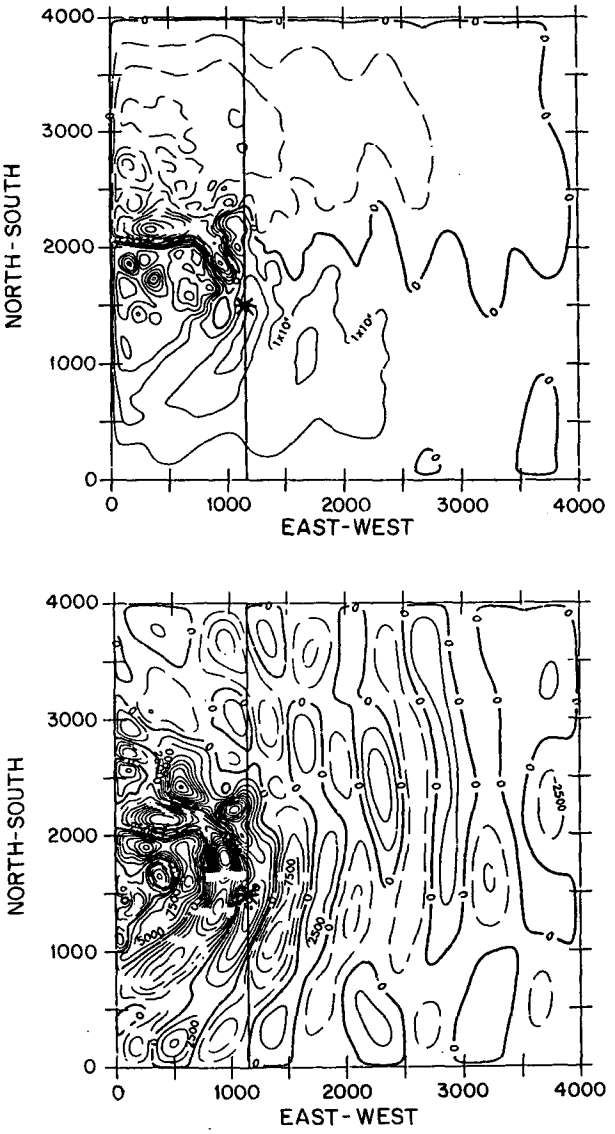

FIG. 5. (Upper) Map of the upper layer streamfunction on day 4. The solid line indicates the position of the tomographic section (x = 1160 km) and the asterisk marks the location of station 1 where the sea surface elevation and currents are computed (y = 1500 km). Contour interval is 1×10^4 m^2 s^{-1} and the dashed lines correspond to negative values. (Bottom) Same except for the lower layer. The contour interval is 0.25×10^4 m^2 s^{-1}.

The three spectra exhibit a broad peak centered near 0.025 cpd (40 day period), and are similar to Miller's results which were obtained with a different 4-year record (see his Figs. 3b, 4e and 5e). The spectrum of the travel time for the 11.7° ray also displays a broadband peak in the same band along with a peak at a period of 29.0 days which is significant at the 95% confidence level (Fig. 8). This peak is also significant at the 95% level in the spectra of the other two rays (not shown).

Is this peak caused by mode 17? We tentatively identify the peak as mode 17 which has a theoretical

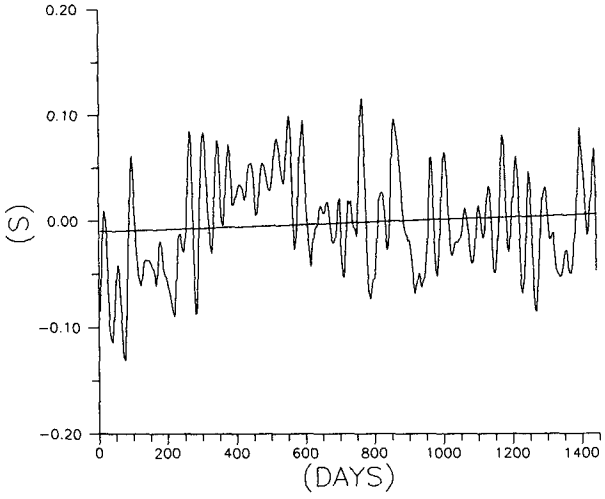

FIG. 6. The entire time series of acoustic travel time change for the 11.7° ray overlaid by the ramp which is used to detrend it.

period of 29.1 days. Using Eq. (12), we calculate the travel time change due to this mode. If we assume the modal energy is spread uniformly in a bandwidth Δf

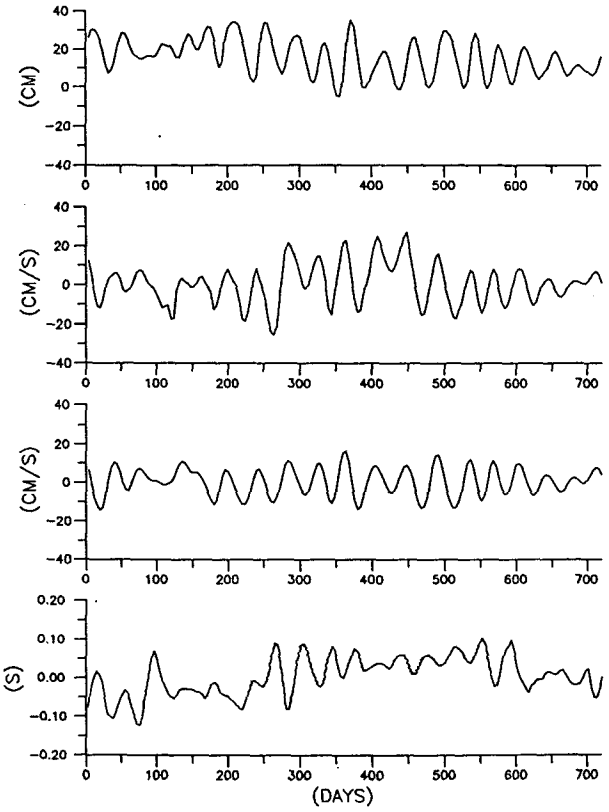

FIG. 7. Time series of sea surface elevation, upper layer meridional current, lower layer meridional current and detrended acoustic travel time change for the 11.7° ray (from top to bottom). Elevation and current are measured at x = 1160 km, y = 1500 km (Fig. 5). The first 2 years of the 4-year records are displayed. The values are computed at 4-day intervals.

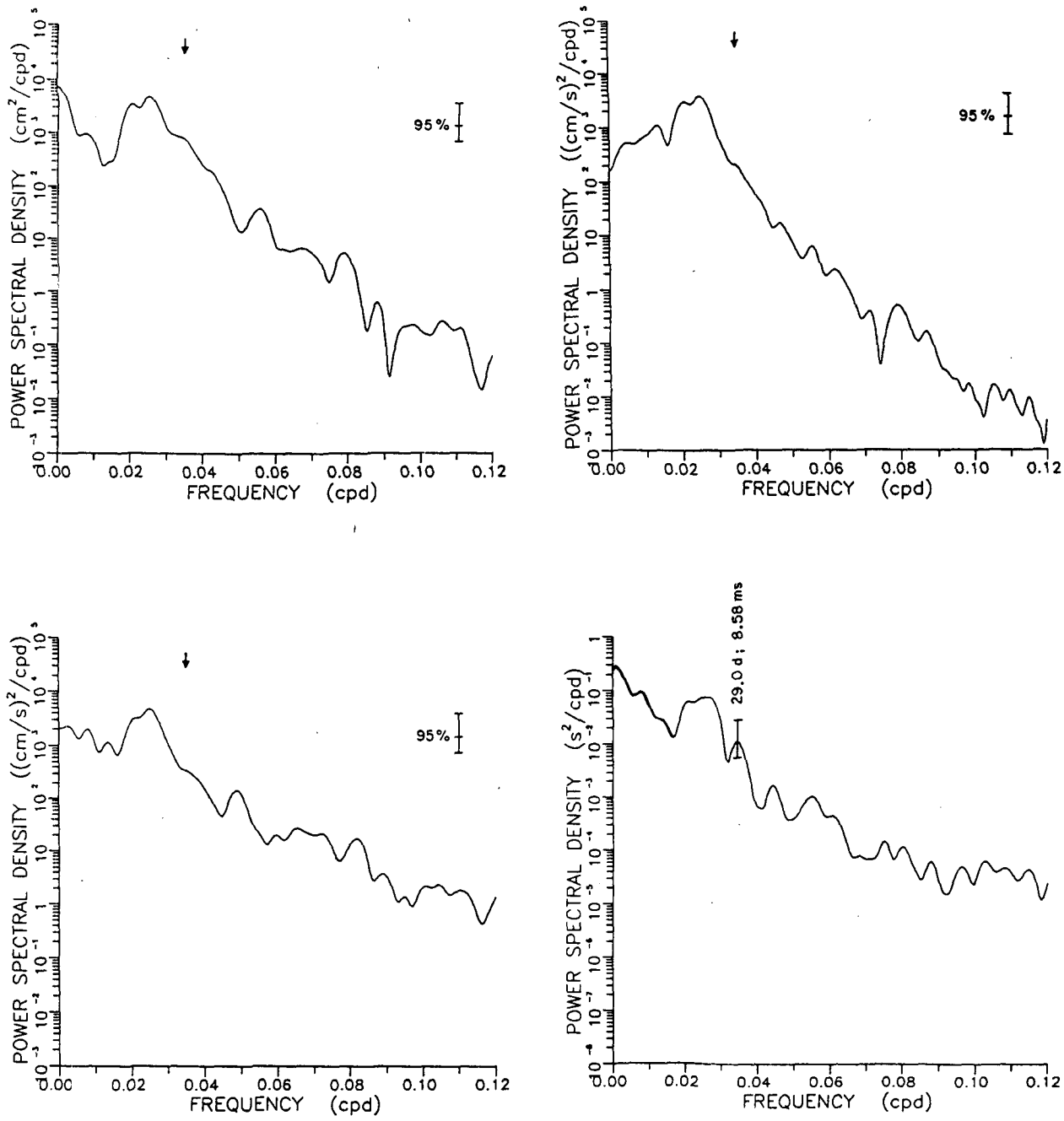

FIG. 8. Power spectral densities of sea surface displacement (upper left) and meridional currents in the upper and lower layers (lower left and upper right) at station 1 and acoustic travel time change for the 11.7° ray (lower right) computed over the 4-year record. In the travel time figure, the period and rms travel time of mode 17 are labeled. In the other figures, the arrow marks the period of the mode. The 95% confidence limits are shown.

(cpd), the power spectral density level P_0 (s^2 cpd^{-1}) is given by

$$P_0 = \frac{\sigma_{\delta t}^2}{\Delta f},$$

where $\sigma_{\delta t}^2$ is the variance of the travel time fluctuation caused by the mode. Table 2 lists the predicted and measured rms travel time and the spectral level for this mode. The predicted spectral level of 3.2×10^{-2} (s^2 cpd^{-1}) is computed using a half-power bandwidth of 0.002 cpd and an amplitude of 1.1 cm which correspond to a Q of about 17 (Miller et al. 1987). The observed spectral level of this peak is about 1.2×10^{-2} (s^2 cpd^{-1}). The predicted and observed levels are similar.

TABLE 2. The predicted values of the rms travel time and the power spectral density are compared with the values computed from the tomographic array. The predicted rms travel time is obtained from Eqs. (11) and (12).

	Rms travel time (ms)	Spectral level (s^2 cpd^{-1})
Predicted	11.27	3.18×10^{-2}
Measured	8.58	1.17×10^{-2}

We seek to determine the influence of the eddy field on the travel times to ensure that the peak is not the result of mesoscale processes. The QG model is high-passed filtered using a Bartlett window. For this filter, wavelengths of 800, 1000 and 2000 km are attenuated by 3.4, 6.1 and 16.0 dB, respectively. Therefore, the mesoscale field is passed and the large-scale planetary modes are attenuated. The averaged periodogram of the travel times is computed over the four-year record for the high-passed model (Fig. 9). The spectral level due to the mesoscale is about 30 dB less than the peak at 29.0 days which is observed in the unfiltered model. Therefore we conclude that the peak at a period of 29.0 days is caused by a planetary basin mode rather than the mesoscale field.

6. Discussion

Although basin-scale resonant barotropic vorticity modes have been detected in numerical models (for example, Willebrand et al. 1980; Miller 1986), attempts to detect this type of motion in the real ocean have not been as successful. Luther (1982) presented the most convincing but, by his own admission, still inconclusive evidence of a barotropic vorticity mode from his analysis of sea level records covering a wide geographic area in the Pacific.

Luther (1983) gives two reasons for the lack of direct observations of basin-scale vorticity modes in the ocean. First, because the modes are weakly excited, their signal may not be strong enough relative to the background noise to be extracted from the data he used. Second, topography can reduce the period and scale of a planetary mode, changing it into a topographic mode that is restricted to the vicinity of the controlling feature.

In this QG model, two factors hinder the observations of barotropic planetary modes in the sea surface and current records. First, the mesoscale field masks the signals of the modes in the point measurements. Second, because the modes are closely spaced in frequency, the presence of friction and nonlinearities can cause the narrow modal peaks to broaden into a broadband peak (Phillips 1966; Miller 1986). However, the tomographic system is not as strongly affected by these factors. A basin-scale tomographic array attenuates the signals from the mesoscale processes so that a mode with a period near 29.0 days can be detected at the 95% confidence limit for a record length of four years. In other words, the acoustic travel time is given by a spatial integral between the source and the receiver which preferentially attenuates the short wavelengths in the ocean (Spiesberger et al. 1989a). Also, tomographic measurements can enhance the signal from an individual mode by locating the section at a position where the modal current has a maximum value.

The location of the current meters in the QG model are optimized to see the 29.0 day mode because they are placed along the same north–south line as the tomographic section where the north–south current is a maximum. If a large enough current meter array was placed along this line, it might detect the mode, but an advantage of tomography is that only a single source–receiver pair is required because of the integrating nature of the measurement.

Spiesberger et al. (1989a,b) have demonstrated that the acoustic phase of the tomographic signals might be used to make estimates of relatively slow barotropic currents whose length scales are large (order of 1000 km or more). No one knows what the spectra of acoustic travel times over basin-scale distances look like for periods greater than a few days. However, the internal wave field imposes a limit. Using one-year records from a tomographic array consisting of one source and ten receivers at about 4000 km range, the threshold at which a periodic basin-scale current can be detected with a confidence of 95% is given by $u \approx 0.034T$ cm s^{-1} where the period of the oscillation, T, is expressed in days (Spiesberger et al. 1989a). For mode 17, T is 29 days, and the threshold speed is 0.1 cm s^{-1}. The amplitude of the mode 17 current in this QG model is 1.0 cm s^{-1} and its Q is about 10, so it oscillates for approximately $10 \times 29 = 290$ days (roughly one year). Therefore, if internal waves limit the precision of the

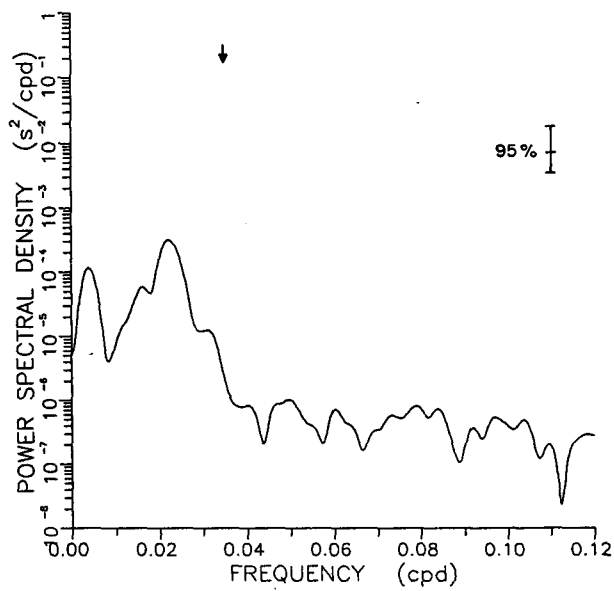

FIG. 9. The power spectral density of acoustic travel time change for the 11.7° ray traveling through the eddy field (but not the large-scale field). The arrow marks the period of mode 17, and the 95% confidence limit is shown.

tomographic array and the real ocean contains modes whose scales are similar to those in the QG model, then the modes would be detected by the tomographic system.

There is a bias in the acoustic travel times due to the mesoscale and the internal wave fields (Spiesberger 1985a,b; Codona et al. 1985). In other words, the travel time for any ray path is lengthened or shortened by a nearly constant amount due to the presence of these fluctuations. If the mesoscale and internal wave spectra are stationary in the statistical sense, then the biases will have no effect on the acoustic travel time changes. However, if the spectra change, then the change in the travel time bias will appear in a series of travel time changes. The bias for each ray path in the Northeast Pacific over a range of 4000 km is of order ±10 ms for eddy perturbations of about 0.5°C (Spiesberger 1985a). If the power in the mesoscale spectrum increases by a factor of two, then the bias increases by a factor of four and the bias is of order ±40 ms. The change in the bias is $\pm(40 - 10) = \pm 30$ ms. When the phase and the amplitude of N ray paths are used to estimate the average acoustic travel time change over all the rays (Spiesberger et al. 1988b), the average change in the travel time bias is reduced to order $30/\sqrt{N}$ ms because the sign of the bias is either positive or negative for any ray. For 4000 km length transmissions in the northeast Pacific, there are about $N = 100$ ray paths (Spiesberger 1988b), so the changing biases lead to an effect of order 3 ms. This variance would appear in the spectrum of acoustic travel times in the frequency band in which the change in the mesoscale energy fluctuates. For example, if the energy changes seasonally, then the change in the bias would have little effect on the detection of the 29.0 day mode observed in this QG model. We conclude that the change in the bias is smaller than the rms travel time change associated with the 29.0 day mode (8.58 ms) and that the variance associated with the bias will probably appear at longer periods and not affect the detection of the mode. Similar arguments can be made for the biases associated with the internal wave field, except the biases may exceed those due to the mesoscale by a factor of about five to ten at this range (Flatte, personal communication). The detection of the barotropic modes may or may not be hindered by the biases depending on the frequency band associated with the energy changes in the internal wave spectrum.

The resonant linear modes have been observed to be excited in two and three layer QG models even when random roughness or a midocean ridge is included in the basin or when the free jet penetrates half-way into the basin as a consequence of inclusion of a sloping bottom (Miller 1986, appendix B; Miller et al. 1987, p. 270). The amplitudes of the modes are generally smaller but some modes have enhanced amplitudes. The shapes of the modes change due to topography, but any tomographic experimental array could be designed for an optimal response based on numerical predictions. The presence of topography also has the effect of reducing the number of degenerate modes and so it may be easier to resolve some modes in frequency space than is suggested by the flat bottom square QG model. It is likely that a re-evaluation of the tomographic signal in more complicated QG models would show the presence of linear resonant vorticity modes even though point measurements would be too noisy to sense them.

Platzman et al. (1981) have computed the periods of the ocean's modes for the range between 8 and 80 hours. Any experimental program which searches for modes with periods exceeding 80 hours would be greatly enhanced by an extension of the numerical calculations to longer periods. However, at these longer periods, the stratification of the ocean and the nonlinear interaction of the modes with other large-scale currents near the same period may be important both for the interpretation of the data and for a reliable numerical computation of the modal structure.

Acknowledgments. This work was partially supported by the Office of Naval Research under Contract N00014-86-C-0358. We thank Art Miller (SIO) for the use of his numerical data which was generated using the Holland model with supercomputing resources from the SIO Block Grant at the San Diego Supercomputer Center. His knowledge of the model's dynamics proved to be very helpful. We also thank Gunnar Roden for permission to use his Pacific Ocean sound speed section. Wendy Lawrence thanks the United States Navy for the opportunity to pursue graduate education through the MIT/WHOI Joint Program.

REFERENCES

Bushong, P. J., 1987: Tomographic measurements of barotropic motions. Masters thesis, Woods Hole Oceanographic Institution–Massachusetts Institute of Technology, 48 pp.

Codona, J., D. Creamer, S. Flatte, R. Frehlich and F. Henyey, 1985: Average arrival time of wave pulses through continuous random media. *Phys. Rev. Lett.*, **55**(1), 9–12.

Holland, W. R., 1978: The role of mesoscale eddies in the general circulation of the ocean—numerical experiments using a wind-driven quasi-geostrophic model. *J. Phys. Oceanogr.*, **8**, 363–392.

Jenkins, G. M., and D. G. Watts, 1968: *Spectral Analysis and Its Applications.* Holden-Day, 525 pp.

Luther, D. S., 1982: Evidence of a 4–6 day barotropic, planetary oscillation of the Pacific Ocean. *J. Phys. Oceanogr.*, **12**, 644–657.

——, 1983: Why haven't you seen an ocean mode lately? *Ocean Modelling*, **50**, 1–6.

Miller, A. J., 1986: Barotropic planetary-topographic oscillations in ocean basins. Ph.D. thesis, University of California, San Diego, 133 pp.

——, W. R. Holland and N. C. Hendershott, 1987: Open-ocean response and normal mode excitation in an eddy-resolving general circulation model. *Geophys. Astrophys. Fluid Dyn.*, **37**, 253–278.

Munk, W. H., 1974: Sound channel in an exponentially stratified ocean, with application to SOFAR. *J. Acoust. Soc. Amer.*, **55**, 220–226.

——, P. Worcester, and F. Zachariasen, 1981: Scattering of sound by internal wave currents: The relation to vertical momentum flux. *J. Phys. Oceanogr.*, **11**, 442–454.

Oppenheim, A. V., and R. W. Schafer, 1975: *Digital Signal Processing*. Prentice-Hall, 585 pp.

Pedlosky, J., 1979: *Geophysical Fluid Dynamics*. Springer-Verlag, 624 pp.

Phillips, N. A., 1966: Large-scale eddy motion in the western Atlantic. *J. Geophys. Res.*, **71**, 3883–3891.

Platzman, G. W., G. A. Curtis, K. S. Hansen and R. D. Slater, 1981: Normal modes of the world ocean. Part II: Description of modes in the period range 8 to 80 hours. *J. Phys. Oceanogr.*, **11**, 579–603.

Roden, G. I., 1984: Mesoscale sound speed fronts in the central and western North Pacific and in the emperor seamounts region. *J. Phys. Oceanogr.*, **14**, 1659–1669.

Schmitz, W. J., and W. R. Holland, 1982: A preliminary comparison of selected numerical eddy-resolving general circulation experiments with observations. *J. Mar. Res.*, **40**, 75–117.

Spiesberger, J. L., 1985a: Ocean acoustic tomography: travel time biases. *J. Acoust. Soc. Amer.*, 77(1), 83–100.

——, 1985b: Gyre-scale acoustic tomography: biases, iterated inversions, and numerical methods. *J. Geophys. Res.*, **90**(C6), 11 869–11 876.

——, P. J. Bushong, K. Metzger, and T. G. Birdsall, 1989a: Basin-scale tomography: Synoptic measurements of a 4000 km length section in the Pacific. *J. Phys. Oceanogr.*, in press.

——, ——, ——, and ——, 1989b: Ocean acoustic tomography: estimating the acoustic travel time with phase. *IEEE J. Ocean. Eng.*, **14**(1), 108–119.

Willebrand, J., S. G. H. Philander and R. C. Pacanowski, 1980: The oceanic response to large-scale atmospheric disturbances. *J. Phys. Oceanogr.*, **10**, 411–429.

Worthington, L. V., 1976: On the North Atlantic circulation. The Johns Hopkins Oceanographic Studies, Rep. No. 6, 110 pp.